Can strong substorm-associated MeV electron injections be an important cause of large radiation belt enhancements?

Hee-Jeong Kim[1]*, S. J. Noh[2,3], D. Y. Lee[4], L. Lyons[1], J. Bortnik[1], T. Nagai[5], W. Choe[6] and M. Hua[1]

[1]Department of Atmospheric and Oceanic Sciences, University of California, Los Angeles, CA, United States, [2]Center for Solar-Terrestrial Research, New Jersey Institute of Technology, Newark, NJ, United States, [3]Los Alamos National Laboratory, Los Alamos, NM, United States, [4]Department of Astronomy and Space Science, Chungbuk National University, Cheongju, Republic of Korea, [5]Retired, Tokyo, Honshu, Japan, [6]May & June Solutions, Seoul, Republic of Korea

It has become well-established that strong outer radiation belt enhancements are due to wave-driven electron energization by whistler-mode chorus waves. However, in this study, we examine strong MeV electron injections on 10 July 2019 and find substantial evidence that such injections may be a crucial contributor to outer radiation belt enhancement events. For such an examination, it is essential to precisely separate temporal flux changes from spatial variations observed as Van Allen Probes move along their orbits. Employing a new "hourly snapshot" analysis approach, we discover unprecedented details of electron flux evolutions that suggest that for this event, the outer belt enhancement was not continuous but instead intermittent, mostly composed of 4 large discrete injection-driven flux increases. The injections appear as sharp flux increases when observed near apogee. Otherwise, by comparing hourly snapshots for different times, we infer injections and infer temporally stable fluxes between injections, despite strong and continuous chorus emission. The fast and intermittent electron flux growth successively extending earthwards implies cumulative outer belt enhancement *via* a series of repetitive inward transport associated with injection-induced electric fields.

KEYWORDS

earth's radiation belts, relativistic electron enhancement, MeV electron injections, rapid radial transport, radial acceleration, substorm injections

1 Introduction

Sudden large relativistic electron enhancements in the outer radiation belt have been observed during not only strong magnetic storms but also during non-storm time intervals (e.g., Meredith et al., 2002; Schiller et al., 2014; Kim et al., 2015; Anderson et al., 2015), as long as there were intense substorms occurring with low solar wind number density (e.g., Kim et al., 2015; Pinto et al., 2018). Currently, local energization *via* repeated gyro-resonant interactions with whistler-mode chorus waves (e.g., Summers et al., 1998; Horne et al., 2005; Thorne et al., 2013) is considered to be the primary cause of such enhancements. However, while receiving far less attention, rapid injections of relativistic electrons from the magnetotail associated with strong substorm
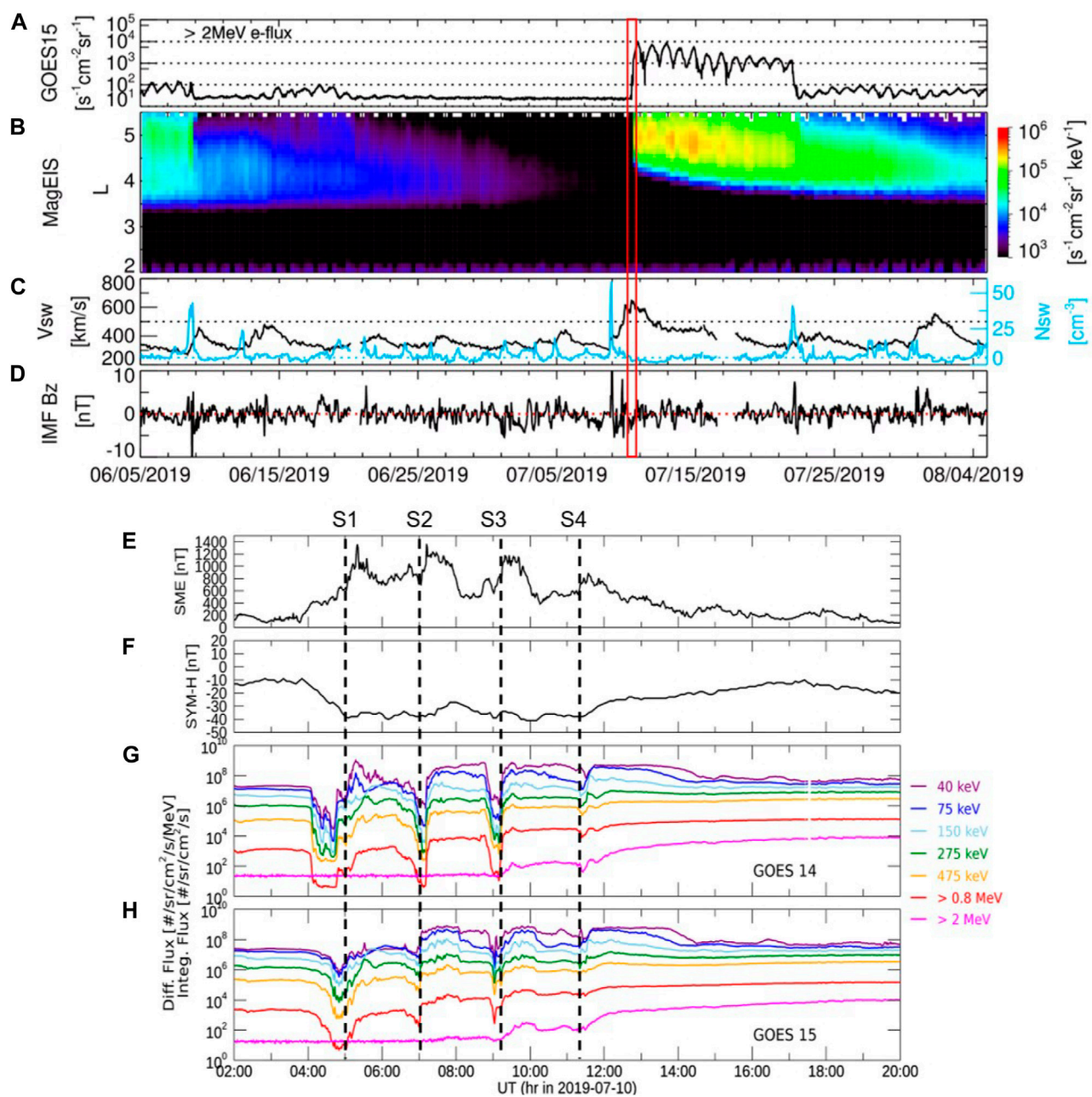
FIGURE 1
(A–D) > 2 MeV electron flux from GOES 15, L-time plot of 2.27 MeV electron flux from MagEIS (Magnetic Electron Ion Spectrometer; Blake et al., 2013) instrument, Vsw and Nsw, and IMF Bz, respectively, for June 5 to 4 August 2019. **(E–H)** SME, SYM-H, electron fluxes for various energies from GOES 14 and 15, respectively, for 02-20 UT on July 10 which correspond to the time interval in red box in **(A–D)**. Dotted lines labeled S1 to S4 indicate the start of 4 intense substorms.

dipolarizations have been suggested to make a significant contribution to radiation belt enhancements from both observations (e.g., Ingraham et al., 2001; Nagai et al., 2006; Nagai, 2012; Dai et al., 2014, 2015; Xiong et al., 2022) and modeling (Kim et al., 2000; Fok et al., 2001; Glocer et al., 2011; Sorathia et al., 2018). Despite these efforts, the possibility that injections can be a major contributor to relativistic electron enhancements is mostly not seriously considered by the community relative to wave-driven energization.

Recently, Kim et al. (2021), hereafter referred to as Paper 1, examined two events exhibiting distinctly-isolated MeV electron injections observed by the Van Allen Probes (Mauk et al., 2013). Employing a new "hourly snapshot" analysis approach, Paper 1 quantified how the entire outer belt responded to the injections. For both events, they discovered extremely-fast (~30-min timescales), large (~1-2 orders of magnitude for ~2 MeV fluxes), step-like outer belt enhancements that occurred 1) promptly and discretely with the injections, 2) simultaneously at

10s–100 s keV to multi-MeV, 3) having an enhancement inner boundary located farther out with increasing energy, consistent with the well-known energy-dependent substorm injection boundary (e.g., Pfitzer & Winkler, 1968; Reeves et al., 2016). The 'fast', 'prompt', and 'discrete' pattern of the enhancements 'simultaneously' over a wide energy range, with the 'energy-dependent inner boundary' are together difficult to explain by the local wave energization, including in combination with radial diffusion, but can be fully attributed to injections. Their findings indicate that even single strong injections can lead to significant outer belt enhancements, supporting the earlier suggestions mentioned above.

Motivated by the findings in Paper 1, here we investigate whether a series of such strong relativistic electron injections can be a crucial contributor to large radiation belt enhancement events. This requires examination of events where each strong injection in a series is well isolated, allowing identification, if any, of injection-driven enhancements characterized by the above-outlined features. Another requirement is no significant flux decreases during the entire course of the event, allowing reliable estimation of the total contribution of the injections. In this study, we adopt the same approach as in Paper 1 and examine one remarkably rapid and large outer belt enhancement event satisfying those conditions.

2 Rapid and intermittent outer belt enhancement on 10 July 2019

2.1 Event overview

Figure 1 presents outer-radiation belt electron fluxes and solar wind parameters for June 5 to 4 August 2019. In Figure 1A, GOES 15 suddenly observed ~3 orders of magnitude increase of >2 MeV flux in less than half a day on July 10 (red box) after the prolonged, nearly background state. Concurrently, in Figure 1B, Van Allen Probes observed rapid enhancement of 2.27 MeV fluxes over a wide region of the outer belt. Figures 1C, D show a high-speed solar wind stream with low number density, and predominantly southward IMF, a typical condition for relativistic electron enhancement events.

For a more detailed view of the GOES's abrupt enhancement, Figures 1E–H present SME (SuperMAG auroral Electrojet index; Newell and Gjerloev, 2011), SYM-H, and electron fluxes from GOES 14 and 15, respectively, during 02–20 UT on July 10. The event occurred during a weak magnetic storm (minimum SYM-H = ~-40 nT), with a series of 4 intense substorms S1 to S4 (dotted lines) that were fairly well-separated, occurring roughly every 2-h and each sustained for ~1-h. In Supplementary Figure S1, these substorms are also identified from sharp drops in the ground magnetic field H-component (negative bays due to westward electrojet of substorm wedge current) and geosynchronous magnetic field dipolarizations. In Figures 1G, H, for each substorm, both GOES 14 and GOES 15 located at nightside MLTs (see Supplementary Figure S2) observed dispersionless or slightly dispersed large flux increases, indicating strong injections of electrons of 10 s keV to relativistic energies into the geosynchronous region (note that >2 MeV fluxes were below the background levels before substorm S3, so that any enhancement at S1 and S2 could not

be seen). We investigate how important these injections are for outer belt enhancement.

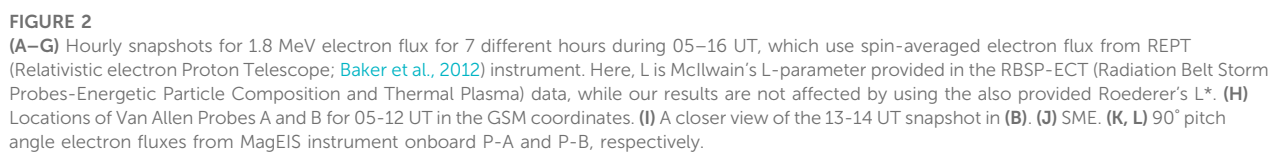## 2.2 Detailed outer belt evolution observed by Van Allen Probes

To accurately interpret electron flux dynamics recorded by Van Allen Probes, it is essential to separate temporal flux changes from spatial variations observed as satellites move along their orbits (i.e., orbital effect). For the separation, the hourly snapshot technique from Paper 1 allows us to simultaneously track electron flux changes observed by both Van Allen Probes A (P-A) and B (P-B), plotting them together as flux versus L over 1-h intervals sequentially advanced by 1-h time-steps, while keeping previous traces on the plot. With this technique, we analyze detailed electron flux evolutions, particularly focusing on identification of significant flux enhancements directly due to the injections in Figure 1.

Due to orbital effects, identification of injection-driven flux increases highly depends on satellites' locations at the injection time. For example, they can be more easily identified if observed near apogee where satellites move slowly, limiting the effect of spatial variations on electron fluxes so that impulsive temporal flux enhancements appear prominent. For this event, both P-A and P-B were located near apogee (~12 MLT) only for substorm S4 (~11:20 UT), as indicated in Figure 2H. Hence, we first examine the well-observed electron flux dynamics for S4, followed by examinations for the earlier substorms; Figure 2 presents hourly snapshots of 1.8 MeV spin-average electron flux for selected hours during 05–16 UT, where the snapshots for substorm S4 are displayed first. In each snapshot, blue (light blue) and pink (light pink) denote the electron flux traces for the current (previous) 1-h observed by P-A and P-B, respectively, while gray denotes the earlier hours since 00 UT on July 10 for both satellites. Supplementary Movie S1 shows the complete sequential snapshots for 00-16 UT, along with the satellites' positions where P-B closely followed P-A on nearly identical, near-equatorial, highly-elliptical orbits.

2.2.1 Step-like flux enhancement associated with substorm S4

In the 11-12 UT snapshot (Figure 2A), outbound P-B (pink; arrow 1) and inbound P-A (blue; arrow 2) started to observe a sudden flux increase at ~11:20 UT. This flux jump is well-timed with substorm S4 (Figure 1E), indicating its immediate occurrence with the injections. The 11-12 UT snapshots for various energies (Figure 3E) show that the increase occurred simultaneously at all energies up to 4.2 MeV. In fact, the time series plots in Figures 2K, L show that the increase is dispersive in the noon sector (red arrows at S4; see Supplementary Figure S3B for more details), consistent with the slightly dispersed increases in the dawn sector observed by GOES (Figures 1G, H). This flux enhancement is not just a simple adiabatic effect (e.g., the Dst effect in Kim and Chan, 1997), as indicated by the corresponding phase space density increase in Section 2.3.

Luckily, we can deduce the completion time of this increase by tracking further in time. In the 13-14 UT snapshot (Figure 2B),

FIGURE 2
(A–G) Hourly snapshots for 1.8 MeV electron flux for 7 different hours during 05–16 UT, which use spin-averaged electron flux from REPT (Relativistic electron Proton Telescope; Baker et al., 2012) instrument. Here, L is McIlwain's L-parameter provided in the RBSP-ECT (Radiation Belt Storm Probes-Energetic Particle Composition and Thermal Plasma) data, while our results are not affected by using the also provided Roederer's L*. **(H)** Locations of Van Allen Probes A and B for 05-12 UT in the GSM coordinates. **(I)** A closer view of the 13-14 UT snapshot in **(B)**. **(J)** SME. **(K, L)** 90° pitch angle electron fluxes from MagEIS instrument onboard P-A and P-B, respectively.
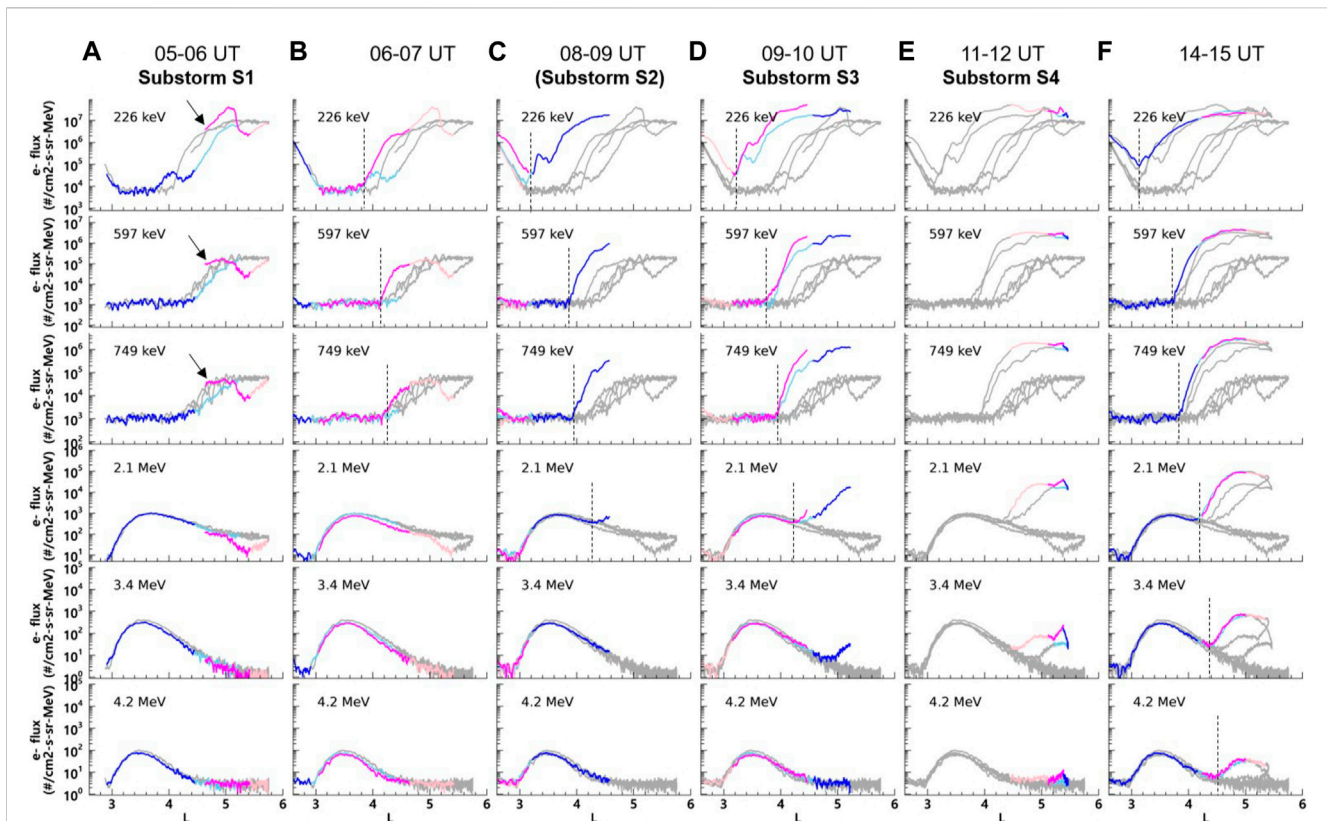
FIGURE 3
(A–F) Hourly flux snapshots for various energies from 226 keV to 4.2 MeV for six different hours.

arrow 3 denotes the starting point (L~5.2) of the overlap of pink (P-B) and light blue (P-A). That is, when inbound P-B, which was roughly 1-h behind P-A, arrived at L~5.2, it started to observe the same flux values that P-A observed earlier at the same L-shells. This overlap-starting point thus indicates no significant temporal flux changes after P-A passed L~5.2. In a closer view in Figure 2I, P-A passed L~5.2 at ~12:30 UT (arrow 3), i.e., the flux increase starting at ~11:20 UT (Figure 2A) ended at ~12:30 UT. Meanwhile, P-B was located at apogee at ~12:30 UT (arrow 3′), and thus observed already-increased fluxes during its new inbound pass, as evidenced from the pinkish above light blue up to the overlap-starting point. Figure 2C shows that P-A's and P-B's traces continued to overlap until ~16 UT, indicating the quasi-stationary outer belt for ~12:30-16:00 UT. Accordingly, the upper-most traces (top gray and pinkish) represent the quasi-stationary spatial flux profile formed at the enhancement completion at S4.

While the flux increases sharply started and ended simultaneously at all energies in Figure 3E, the inner-most L of the flux increase (dotted lines; Figure 3F) is energy-dependent, located farther out with increasing energy. As clearly demonstrated in Paper 1, such energy dependency is consistent with the energy-dependent substorm injection boundary (e.g., Pfitzer and Winkler, 1968; Reeves et al., 2016). The step-like flux increase at substorm S4 thus exhibits all the characteristic features of injection-driven enhancement reported in Paper 1, i.e., prompt,

discrete, and simultaneous over a wide energy range with energy-dependent inner boundary.

2.2.2 Quasi-stationary state for ~10:00-11:20 UT

In Figure 1, during the time interval (~10:00-11:20 UT) between substorms S3 and S4, SME is relatively low (~500 nT) without strong injections at GOES. The flux traces during this period, i.e., blue and pink in the 10-11 UT snapshot (Figure 2D and some of Figure 2A), suggest that the outer belt was also stable before the impulsive enhancement at substorm S4. In Figure 2D, comparison of the blue and light blue shows drastic change in the flux radial gradients at ~10 UT, i.e., from increasing to slightly decreasing flux with increasing L (dotted line with arrow 4), indicating no more flux increases for L > 5.2 for 10-11 UT. Comparably, when P-B moved out to L~4.9 at ~10:35 UT (arrow 5), it started to observe the same, slightly negative gradients until arriving at L~5.2 at 11:20 UT where P-B observed the nearly same flux that P-A observed earlier (10 UT). These observations indicate that fluxes were temporally-stable during ~10:00-11:20 UT at least for L ≳ 4.9. As argued later, the P-B's flux increase for 10-11 UT in Figure 2D (i.e., pink above light blue) is attributable to the injection by earlier substorm S3 (09:10-10:00 UT, Figure 2G), suggesting that the pink trace (even for L < 4.9) is spatial. Thus, both pink and blue in Figure 2D represent the quasi-stationary flux distribution for L ≳ 4.5 (with a peak at L~4.9) for 10:00-11:20 UT. Note the shape similarity between this and the new quasi-stationary distribution after substorm S4 (i.e., uppermost gray

and pinkish traces in Figure 2C), which implies monotonic flux enhancement over a wide L-region, likely induced by a coherent electron response to substorm S4. The observation of stable fluxes during the absence of strong injections before and after the impulsive enhancement at S4 suggests a direct relationship between injections and flux enhancements even for MeV energies.

The lesser importance of chorus wave acceleration (e.g., Thorne et al., 2013) for this event is seen by examination of chorus wave data. As expected under the series of substorm injections, chorus waves (with average amplitudes (B_w) of ~50 pT and sporadic peaks up to 200 pT) were frequently observed for 08-16 UT in Supplementary Figure S4 (note the unfavorable satellites' local times for chorus wave observation). In particular, during 10:00-11:20 UT, large-intensity chorus waves (average B_w ~ 115 pT) were observed by P-A for L≥5.2. It has been suggested that such strong chorus waves can drive non-linear effects and accelerate electrons much faster than quasi-linear interaction (Albert, 2002; Bortnik et al., 2008; Foster et al., 2017). However, as argued above (Figure 2D; arrow 4), the electron fluxes at L≥5.2 barely increased during 10:00-11:20 UT, indicating little enhanced chorus wave acceleration. Furthermore, the primarily injection-driven flux enhancement at substorm S4 (Figure 2A) and the quasi-stationary fluxes for ~12:30-16:00 UT (Figure 2C), both occurring under fairly strong and continuous chorus waves, are inconsistent with wave acceleration dominating. These indicate that the relativistic electron intensities for ~10-16 UT were mainly governed by injections, not by chorus acceleration.

Next, we examine whether the electron fluxes during earlier substorms S1 to S3 were also mainly driven by injections. For the examination, we emphasize: First, based on the elucidated flux dynamics during, before, and after substorm S4, it is reasonable to speculate that similar injection-driven enhancements may have occurred for comparably (or more) intense S1 to S3, with stable fluxes for the much weaker activity intervals (as marked by lower SME and lack of strong GOES injections) in-betweens. Second, due to the satellites' more earthward locations (larger spatial effect), injections for S1 to S3 would appear more gradual than impulsive.

2.2.3 Flux increase associated with substorm S1

In Figure 1, after rapid Dst drop for ~04-05 UT, which yielded large flux decreases, substorm S1 occurred with strong injections at GOES. Correspondingly, in the 05-06 UT snapshot (Figure 2E), inbound P-B (light pink) observed a large flux decrease starting at ~04 UT (arrow 6). Note the simultaneous P-A's (light blue) observation of little flux decrease at lower L-shells. Then, P-B started to observe flux increase (arrow 7) several minutes after the injections at 5 UT. Note that we cannot determine whether or how much 1.8 MeV electron flux increased for ~05-06 UT, because the light pink in Figure 2E indicates temporally-ongoing flux decrease, while pink might indicate temporally-ongoing flux increase. That is, we have no information on how much flux decreased in total at L > 5 during 04–05 UT and how much it increased there during 05–06 UT. From the overlap of gray, light blue, and pink at L~4.6-5.0, we can at best deduce that 1.8 MeV electron flux at L < 5 did not change significantly during 04–06 UT. In contrast; Figure 3A clearly indicates simultaneous flux increase at ≤749 keV (pink above light blue; arrows). During the next 1-h, P-B (Figure 3B, pink) continued to observe larger fluxes for ≤749 keV in the outer
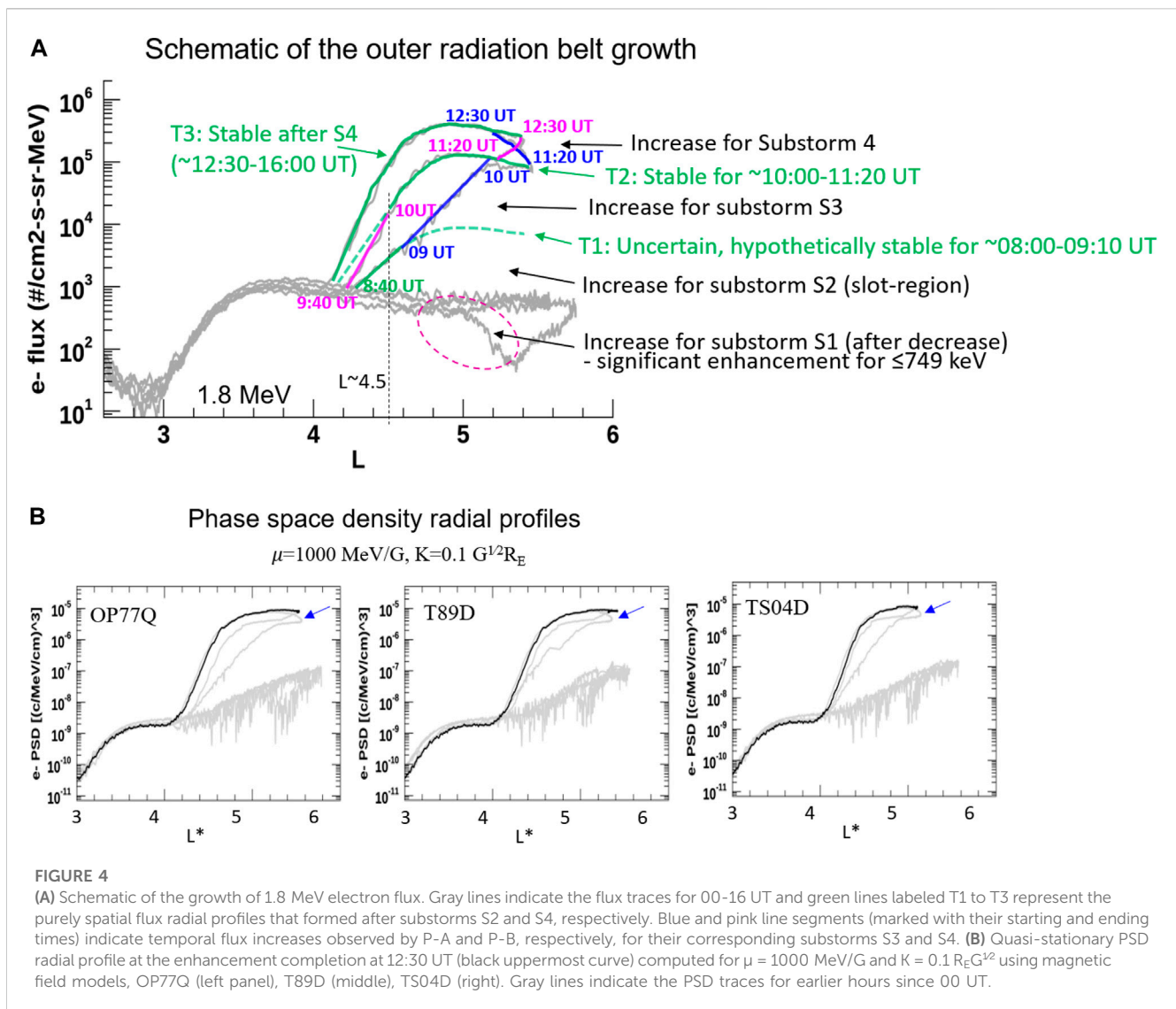
belt region. Although this observation alone cannot determine when the flux increase ended (however, note the absence of strong injection signatures for ~06-07 UT), the observation reveals an important injection feature, i.e., the inner-most L of flux increase (dotted lines) is located farther out with increasing energy, consistent with the energy-dependent injection boundary, as noted in Figure 3F. This and the simultaneous flux increase at ≤749 keV immediately with injections suggest that the flux enhancement for ~05 UT to (sometime before) 07 UT is likely primarily caused by nightside injections at substorm S1.

2.2.4 Flux increase associated with substorm S2

During substorm S2 (~07-08 UT; Figure 2H), both satellites were mostly inside the slot region and thus could not observe any ongoing flux increase. In the 08-09 UT snapshot (Figure 2F), P-A moved out to the outer belt, and at ~08:40 UT (arrow 8) it started to observe larger fluxes than previously observed (blue above gray). This observation does not necessarily mean that flux increase started at ~08:40 UT, i.e., from just the blue trace, we cannot determine whether P-A was observing temporally-ongoing increase or previously-occurred (spatial) increase. Although the exact timing of this increase cannot be confirmed, GOES observations and SME time profile in Figure 1 provide an indication of when it occurred. In Figures 1G, H, with substorm S2, GOES observed sudden large flux enhancement at 07 UT (the step-like feature is remarkable for GOES 15) which occurred simultaneously at all energies for up to >0.8 MeV. Following this, a much weaker activity interval persisted for 08-09 UT, until another sharp and large enhancement occurred with substorm S3. The temporal patterns of the GOES electron flux and SME during this weaker activity interval closely resemble those observed during the 10:00-11:20 UT when temporal stability in electron fluxes was demonstrated earlier. This resemblance suggests that electron fluxes may have been also likely stable during 08–09 UT. In addition, Figure 3C shows that outbound P-A started to observe flux increase (dotted lines) at later times with increasing energy up to 2.1 MeV. This is likely the spatial effect of an energy-dependent inner boundary from a prior injection during substorm S2, as similarly seen after substorm S4 (Figure 3F), during which a simultaneous increase was seen at higher L for all energies (Figure 3E). Taking all these observations into account, we interpret the flux increase in Figure 2F as being what occurred earlier during ~07–08 UT due to injections at substorm S2.

2.2.5 Flux increase associated with substorm S3

In the 09-10 UT snapshot (Figure 2G), P-B also moved out to the outer belt, and at ~09:40 UT (arrow 9) it started to observe larger fluxes than what P-A observed during the previous hour (pink above light blue), indicating flux enhancement between the observation times of the pink and light blue at each L (e.g., gray vertical line with a red arrow denotes the enhancement at L~4.5 for 09-10 UT). Meanwhile, P-A at higher L continued to observe increasing flux (arrow 10). Concurrently with the growing flux at lower L (pink above light blue), the fluxes at higher L (blue) are also most-likely temporally increasing. The followings support that this increase is injection. First, corresponding to the injections at S3, in Figure 2K (more

FIGURE 4
(A) Schematic of the growth of 1.8 MeV electron flux. Gray lines indicate the flux traces for 00-16 UT and green lines labeled T1 to T3 represent the purely spatial flux radial profiles that formed after substorms S2 and S4, respectively. Blue and pink line segments (marked with their starting and ending times) indicate temporal flux increases observed by P-A and P-B, respectively, for their corresponding substorms S3 and S4. **(B)** Quasi-stationary PSD radial profile at the enhancement completion at 12:30 UT (black uppermost curve) computed for $\mu = 1000$ MeV/G and K = 0.1 $R_E G^{1/2}$ using magnetic field models, OP77Q (left panel), T89D (middle), TS04D (right). Gray lines indicate the PSD traces for earlier hours since 00 UT.

clearly in Supplementary Figure S3A), P-A at higher L observed dispersive flux increase in the pre-noon sector (S3; red arrow). Concurrently, in Figure 3D, P-B at lower L started to observe a flux increase (dotted lines) at later time with increasing energy, i.e., the spatial effect of the energy-dependent injection boundary. The completion time of this increase offers further support. As elaborated earlier in Figure 2D, P-A's observation of the drastic change in flux radial gradients (from light blue to blue) at L~5.2 at ~10 UT and P-A's and P-B's observing roughly the same fluxes at L~5.2 at 10 UT and ~11:20 UT, respectively, as well as observing the steady, slightly negative gradients for ~10:00-11: 20 UT, indicate no more flux increases after ~10 UT. This abrupt ending of the flux increase despite strong chorus waves continuing after 10 UT (Supplementary Figure S4) convincingly supports that the flux enhancement for ~09:10-10:00 UT is predominantly due to injections at substorm S3.

Combining the satellites' locations, SME time profile, and GOES observations, the detailed flux traces in Figures 2, 3 suggest separated, strong flux enhancements at substorms S1 to S4, with quasi-stationary states in-betweens. Importantly, the flux traces did

not indicate any significant flux decreases during the entire course of the event (~05:00-12:30 UT).

2.3 Schematic of the outer radiation belt growth

The schematic in Figure 4A illustrates our interpretation of the growth of 1.8 MeV electron flux during the event. Gray lines indicate the flux traces for 00-16 UT and green lines (overlapping with some grey lines), T1 to T3, represent the quasi-stationary outer belt profiles that formed after substorms S2 to S4, respectively. These profiles are essentially inferred from the temporally-stable fluxes identified earlier. Specifically, for T3, we simply use the upper-most traces in Figure 2C that indicate the quasi-stationary outer belt for ~12:30-16:00 UT after sudden flux enhancement for substorm S4 (see the pink and blue line segments marked with their starting and ending times, i.e., 11:20-12: 30 UT; Figure 4A). Then, T2 is mainly inferred from the observation in Figure 2D that fluxes were stable for ~10:00-11:20 UT after large flux enhancement for substorm S3 (see the pink and blue segments marked

9:40-10 UT and 9-10 UT, respectively; Figure 4A), i.e., T2 for L≳4.5 is simply obtained by combining the flux traces for 10:00-11:20 UT in Figure 2D (and part of Figure 2A). In contrast, T2 for L≲4.5 can only be inferred from the outer belt being enhanced monotonically during the event without any large flux decreases, i.e., T2 should be below T3 and above the pink segment marked 9:40-10 UT. We roughly draw a dotted line as T2 for L≲4.5, making its shape consistent with T3 (here, dashed green lines are inferences from observations, while solid are from direct observations). The shape similarity between T2 and T3 implies that the impulsive flux enhancement for substorm S4 likely occurred throughout L > 4, moving the inner boundary of enhancement to lower L. Lastly, T1 can only be inferred very roughly, representing the stable outer belt for 08-09 UT. In Figure 2F, the blue trace for 08-09 UT is most likely spatial and previously increased for substorm S2. Thus, we use it as T1 for L≲4.6. On the other hand, without information on fluxes at L≳4.6, we can only roughly draw that part of T1, making its shape resemble T2 and T3. The schematic illustrates intermittent outer belt growths, where with each flux enhancement, the inner boundary extended earthwards.

Figure 3 indicates the same pattern of flux growth systematically for all energies, retaining the energy-dependent inner boundary feature. Such growth pattern is consistent with inward radial transport, which is further consistent with the PSD radial profile in Figure 4B. Using the temporally-stable fluxes for ~12:30-16:00 UT, we can estimate quasi-stationary PSD radial profile right at the enhancement completion at 12:30 UT. The black curve in each panel of Figure 4B represents such profile for $\mu = 1000$ MeV/G and $K = 0.1$ $R_E G^{1/2}$ for magnetic field models, OP77Q (Olson and Pfizer, 1977), T89D (Tsyganenko, 1989), TS04D (Tsyganenko and Sitnov, 2005), respectively. Gray lines represent earlier PSD traces since 00 UT, where the sudden PSD jump (arrow) corresponds to the step-like flux enhancement at substorm S4. For all the field models, the PSD radial gradients are outward, indicating inward radial transport. We note that Figure 4B does not cover the entire outer belt, since no adequate data is available for determination of the purely spatial PSD for higher L-regions where there might be a local peak (Boyd et al., 2018). It is noteworthy, however, that in general, for various technical and physical reasons, a local PSD peak is not conclusive evidence for local acceleration (Lejosne et al., 2022). For instance, depending on the pre-existing electron spectra and flux radial gradients before injections or large flux drops at higher L's after injections, we may have locally peaked PSD even for injection-driven enhancements (e.g., Sergeev et al., 1998; Green et al., 2004; Xiong et al., 2022).

3 Conclusion

The present study employs the new hourly snapshot technique to examine the significance of relativistic electron injections for the radiation belt enhancement event where ~2 MeV fluxes increased by ~3 orders of magnitude within a period of 7.5 h. The Van Allen Probes were in relatively good positions to analyze electron responses during and between 4 well-separated, intense substorms (S1 to S4). Our analysis approach overcomes the limitation of rapid radial transport not being accurately

represented by current diffusion-driven radiation belt models (Lejosne et al., 2022) and reveals:

1. For substorm S4, impulsive (i.e., sharply started and ended) flux enhancement and corresponding PSD jump were observed near apogee, this impulsive enhancement likely occurring throughout L > 4, simultaneously at up to 4.2 MeV, exhibiting the lowest-L of enhancement located farther out for higher energy consistent with the energy-dependent substorm injection boundary.
2. For the much weaker activity intervals without strong injections before and after substorm S4, no significant flux enhancements were observed, despite continuous and strong chorus waves.
3. For substorms S1 to S3, the flux enhancements appeared more smooth than impulsive. However, it is expected from the satellites' more earthward locations (larger spatial effects). We identified injection features, including simultaneity over a wide energy range (for ≤749 keV for S1), energy dispersion, and energy-dependent inner boundary consistent with the substorm injection boundary.
4. With each electron flux enhancement, the enhancement successively extended earthwards, maintaining the energy-dependent inner boundary feature.

These observed characteristics of electron enhancement do not align with the conventional understanding of wave acceleration as a primary driver. Instead, they suggest that injections may have played a larger role in this enhancement event. While we do not have direct observations of the impulsive start and end of each enhancement, the integration of Van Allen Probes locations, SME time profile (i.e., recurring intense substorms with much weaker activity intervals in-betweens), and GOES observations support our inferences from the above-listed observations that the overall outer belt enhancement for this event was not continuous but rather composed of 4 discrete episodes at times of strong injections. This pattern is consistent with the cumulative and repetitive rapid inward transport associated with substorm-induced electric fields.

Although we presented only one case, the analysis implies that relativistic electron injections can be a crucial contributor to radiation belt enhancement events. There is the question of whether there are sufficient electrons in the magnetotail to account for the MeV electron intensity in the outer belt *via* adiabatic transport. However, Turner et al. (2021) presented new evidence that at times, there is sufficient population in the central plasma sheet. Finally, how those electrons can be transported into the outer belt remains an important question, a possibility being the injection model of Sorathia et al. (2018).

Data availability statement

Publicly available data sets were analyzed in this study. The data sets can be found here : https://rbsp-ect.newmexicoconsortium.org for Van Allen Probes electron flux data, https://supermag.jhuapl.edu/indices for SME index, http://omniweb.gsfc.nasa.gov/ for solar wind and geomagnetic index, https://satdat.ngdc.noaa.gov/sem/goes/data/ for GOES electron flux and magnetic field data, and https://themis.igpp.ucla.edu for ground magnetic field data.

Author contributions

Funding

Acknowledgments

Conflict of interest

The authors declare that the research was conducted in the absence of any commercial or financial relationships that could be construed as a potential conflict of interest.

Publisher's note

Supplementary material

The Supplementary Material for this article can be found online at: https://www.frontiersin.org/articles/10.3389/fspas.2023.1128923/full#supplementary-material

References

Albert, J. M. (2002). Nonlinear interaction of outer zone electrons with VLF waves. *Geopys. Res. Lett.* 29 (8), 116-1–116-3. doi:10.1029/2001GL013941

Anderson, B. R., Millan, R. M., Reeves, G. D., and Friedel, R. H. (2015). Acceleration and loss of relativistic electrons during small geomagnetic storms. *Geophys. Res. Lett.* 42 (10), 10113–10119. 113–10119. doi:10.1002/2015GL066376

Baker, D. N., Kanekal, S. G., Hoxie, V. C., Batiste, S., Bolton, M., Li, X., et al. (2012). The relativistic electron-proton telescope (REPT) instrument on board the radiation belt storm Probes (RBSP) spacecraft: Characterization of Earth's radiation belt high-energy particle populations. *Space Sci. Rev.* 179, 337–381. doi:10.1007/s11214-012-9950-9

Blake, J. B., Carranza, P. A., Claudepierre, S. G., Clemmons, J. H., Crain, W. R., Dotan, Y., et al. (2013), The magnetic electron Ion spectrometer (MagEIS) instruments aboard the radiation belt storm Probes (RBSP) spacecraft, *Space Sci. Rev.* 179 383, doi:10.1007/S11214-013-9991-8

Bortnik, J., Thorne, R. M., and Inan, U. S. (2008). Nonlinear interaction of energetic electrons with large amplitude chorus. *Geophys. Res. Lett.* 35, L21102. doi:10.1029/2008GL035500

Boyd, A. J., Turner, D. L., Reeves, G. D., Spence, H. E., Baker, D. N., and Blake, J. B. (2018). What causes radiation belt enhancements: A survey of the van allen Probes era. *Geophys. Res. Lett.* 45, 5253–5259. doi:10.1029/2018GL077699

Dai, L., Wang, C., Duan, S., He, S., Wygant, J. R., Cattell, C. A., et al. (2015). Near-Earth injection of MeV electrons associated with intense dipolarization electric fields: Van Allen Probes observations. *Geophys. Res. Lett.* 42, 6170–3881. doi:10.1002/2015GL064955

Dai, L., Wygant, J. R., Cattell, C. A., Thaller, S., Kersten, K., Breneman, A., et al. (2014). Evidence for injection of relativistic electrons into the Earth's outer radiation belt via intense substorm electric fieldsfields. *Geophys. Res. Lett.* 41, 1133–1141. doi:10.1002/2014GL059228

Fok, M. -C., Moore, T. E., and Spjeldvik, W. N. (2001). Rapid enhancement of radiation belt electron fluxes due to substorm dipolarization of the geomagnetic field. *J. Geophys. Res.* 106, 3873–3882. doi:10.1029/2000JA000150

Foster, J. C., Erickson, P. J., Omura, Y., Baker, D. N., Kletzing, C. A., and Claudepierre, S. G. (2017). Van Allen Probes observations of prompt MeV radiation belt electron acceleration in nonlinear interactions with VLF chorus. *J. Geophys. Res. Space Phys.* 122, 324–339. doi:10.1002/2016JA023429

Glocer, A., Fok, M.-C., Nagai, T., Tóth, G., Guild, T., and Blake, J. (2011). Rapid rebuilding of the outer radiation belt. *J. Geophys. Res.* 116, A09213. doi:10.1029/2011JA016516

Green, J. C., Kivelson, M. G., Meredith, N. P., Glauert, S. A., and Smith, A. J. (2004). Relativistic electrons in the outer radiation belt: Differentiating between acceleration mechanismsWave acceleration of electrons in the van allen radiation belts. *J. Geophys. Res.Nature* 109, A03213227–A03213230. doi:10.1029/2003JA010153

Horne, R. B., Thorne, R. M., Shprits, Y. Y., Meredith, N. P., Glauert, S. A., Smith, A. J., et al. (2005). Wave acceleration of electrons in the Van Allen radiation belts. *Nature* 437, 227–230. doi:10.1038/nature03939

Ingraham, J. C., Cayton, T. E., Belian, R. D., Christensen, R. A., Friedel, R. H. W., Meier, M. M., et al. (2001). Substorm injection of relativistic electrons to geosynchronous orbit during the great magnetic storm of March 24, 1991. *J. Geophys. Res.* 106, 25759776–25825776. 759–25. doi:10.1029/2000JA000458

Kim, H. -J., and Chan, A. A. (1997). Fully adiabatic changes in storm time relativistic electron fluxes. *J. Geophys. Res.* 102 (A10), 22107–22116. doi:10.1029/97JA01814

Kim, H. -J., Chan, A. A., Wolf, R. A., and Birn, J. (2000). Can substorms produce relativistic outer belt electrons? *J. Geophys. Res.* 105, 7721–7735. doi:10.1029/1999JA900465

Kim, H.-J., Lee, D.-Y., Wolf, R., Bortnik, J., Kim, K.-C., Lyons, L., et al. (2021). Rapid injections of MeV electrons and extremely fast step-like outer radiation belt enhancements. *Geophys. Res. Lett.* 48. doi:10.1029/2021GL093151

Kim, H.-J., Lyons, L., Pinto, V., Wang, C.-P., and Kim, K. C. (2015). Revisit of relationship between geosynchronous relativistic electron enhancements and magnetic storms. *Geophys. Res. Lett.* 42, 6155–6161. doi:10.1002/2015GL065192

Lejosne, S., Allison, H. J., Blum, L. W., Drozdov, A. Y., Hartinger, M. D., Hudson, M. K., et al. (2022). Differentiating between the leading processes for electron radiation belt acceleration. *Front. Astron. Space Sci.* 9, 896245. doi:10.3389/fspas.2022.896245

Mauk, B. H., Fox, N. J., Kanekal, S. G., Kessel, R. L., Sibeck, D. G., and Ukhorskiy, A. (2013). Science objectives and rationale for the radiation belt storm Probes mission. *Space Sci. Rev.* 179, 3–27. doi:10.1007/s11214-012-9908-y

Meredith, N. P., Horne, R. B., Iles, R. H. A., Thorne, R. M., Heynderickx, D., and Anderson, R. R. (2002). Outer zone relativistic electron acceleration associated with substorm-enhanced whistler mode chorus. *J. Geophys. Res.* 107 (7), 1144. doi:10.1029/2001JA900146

Nagai, T. A. (2012). Rebuilding process of the outer electron radiation belt: The spacecraft akebono observations. *Geophys. Monogr. Ser.* 199, 177–188. doi:10.1029/2012GM001281

Nagai, T. A., Yukimatu, S., Matsuoka, A., Asai, K. T., Green, J. C., Onsager, T. G., et al. (2006). Timescales of relativistic electron enhancements in the slot region. *J. Geophys. Res.* 111, A11205. doi:10.1029/2006JA011837

Newell, P. T., and Gjerloev, J. W. (2011). Evaluation of SuperMAG auroral electrojet indices as indicators of substorms and auroral power. *J. Geophys. Res.* 116, A12211. doi:10.1029/2011JA016779

Olson, W., and Pfitzer, K. (1977). Magnetospheric magnetic field modeling. *Annu. Sci. Rep.* F44, 620–675.

Pfitzer, K. A., and Winkler, J. R. (1968). Experimental observation of a large addition to the electron inner radiation belt after a solar flare event. *J. Geophys. Res.* 73, 5792–5797. doi:10.1029/ja073i017p05792

Pinto, V. A., Kim, H.-J., Lyons, L. R., and Bortnik, J. (2018). Interplanetary parameters leading to relativistic electron enhancement and persistent depletion events at geosynchronous orbit and potential for prediction. *J. Geophys. Res. Space Phys. Space Phys.* 123, 1134–1145. doi:10.1002/2017JA024902

Reeves, G. D., Friedel, R. H. W., Larsen, B. A., Skoug, R. M., Funsten, H. O., Claudepierre, S. G., et al. (2016). Energy-dependent dynamics of keV to MeV electrons in the inner zone, outer zone, and slot regions. *J. Geophys. Res. Space Phys.* 121, 397–412. doi:10.1002/2015JA021569

Schiller, Q., Li, X., Blum, L., Tu, W., Turner, D. L., and Blake, J. B. (2014). A nonstorm time enhancement of relativistic electrons in the outer radiation belt. *Geophys. Res. Lett.* 41, 7–12. doi:10.1002/2013GL058485

Sergeev, V. A., Shukhtina, M. A., Rasinkangas, R., Korth, A., Reeves, G. D., Singer, H. J., et al. (1998). Event study of deep energetic particle injections during substorm. *J. Geophys. Res.* 103 (5), 9217–9234. doi:10.1029/97JA03686

Sorathia, K. A., Ukhorskiy, A. Y., Merkin, V. G., Fennell, J. F., and Claudepierre, S. G. (2018). Modeling the depletion and recovery of the outer radiation belt during a geomagnetic storm: Combined MHD and test particle simulations. *J. Geophys. Res. Space Phys.* 123, 5590–5609. doi:10.1029/2018JA025506

Summers, D., Thorne, R. M., and Xiao, F. (1998). Relativistic theory of wave-particle resonant diffusion with application to electron acceleration in the magnetosphere. *J. Geophys. Res.* 103 (A9), 20487. doi:10.1029/98JA01740

Thorne, R. M., Li, W., Ni, B., Ma, Q., Bortnik, J., Chen, L., et al. (2013). Rapid local acceleration of relativistic radiation-belt electrons by magnetospheric chorus. *Nature* 504, 411–414. doi:10.1038/nature12889

Tsyganenko, N. A. (1989). A magnetospheric magnetic field model with a warped tail current sheet. *Planet. Space Sci.* 37 (5–20), 5–20. doi:10.1016/0032-0633(89)90066-4

Tsyganenko, N. A., and Sitnov, M. I. (2005). Modeling the dynamics of the inner magnetosphere during strong geomagnetic storms. *J. Geophys. Res.* 110, A03208. doi:10.1029/2004ja010798

Turner, D. L., Cohen, I. J., Michael, A., Sorathia, K., Merkin, S., Mauk, B. H., et al. (2021). Can Earth's magnetotail plasma sheet produce a source of relativistic electrons for the radiation belts? *Geophys. Res. Lett.* 48, e2021GL095495. doi:10.1029/2021GL095495

Xiong, S.-L., Dai, L., Wang, C., Wygant, J., Cattell, C., Tao, X., et al. (2022). Relativistic electron enhancements through successive dipolarizations during a CIR-driven storm. *J. Geophys. Res. Space Phys.* 127, e2021JA030088. doi:10.1029/2021JA030088